D-wave superconductivity and charge-density waves in cuprates: Phase diagrams and stationary Josephson currents

Alexander Gabovich, Alexander Voitenko

(*Kiev, Ukraine*)

T. Ekino (*Hiroshima, Japan*)

Mai Suan Li, M. Pękała, H. Szymczak (*Warsaw, Poland*)

Experiment: Angular distribution of gaps and pseudogaps in cuprates

$Bi_{2-y}Pb_ySr_{2-z}La_zCuO_{6+\delta}$

$Bi_2Sr_2CaCu_2O_{8+\delta}$

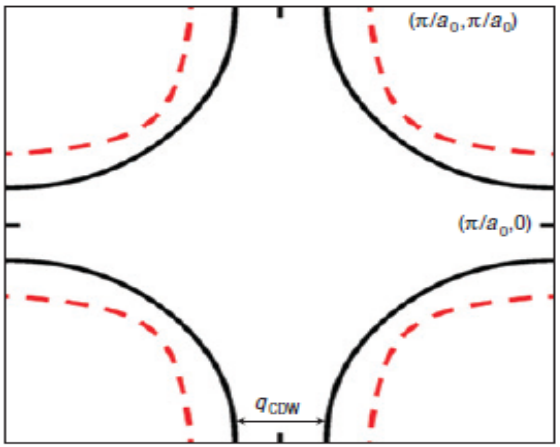

Figure 4 Fermi surface nesting. Tight-binding-calculated Fermi surface (solid black curve) of optimally doped Bi-2201 (ref. 23) based on ARPES data[33]. The nesting wave vector (black arrow) in the antinodal flat band region has length $2\pi/6.2a_0$. Underdoped Bi-2201 Fermi surfaces (shown schematically as red dashed lines) show a reduced volume and longer nesting wave vector, consistent with a CDW origin of the doping-dependent checkerboard pattern reported here.

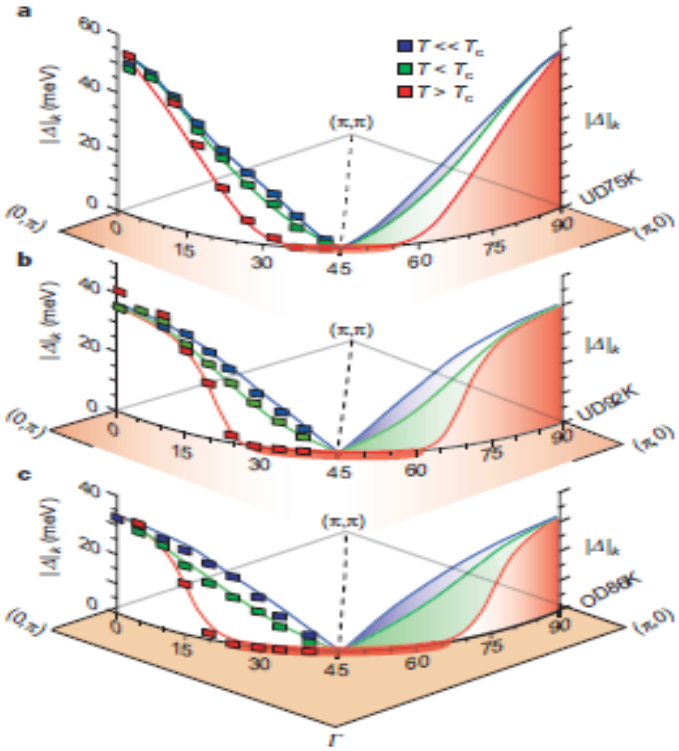

Charge-density wave “checkerboard” modulation

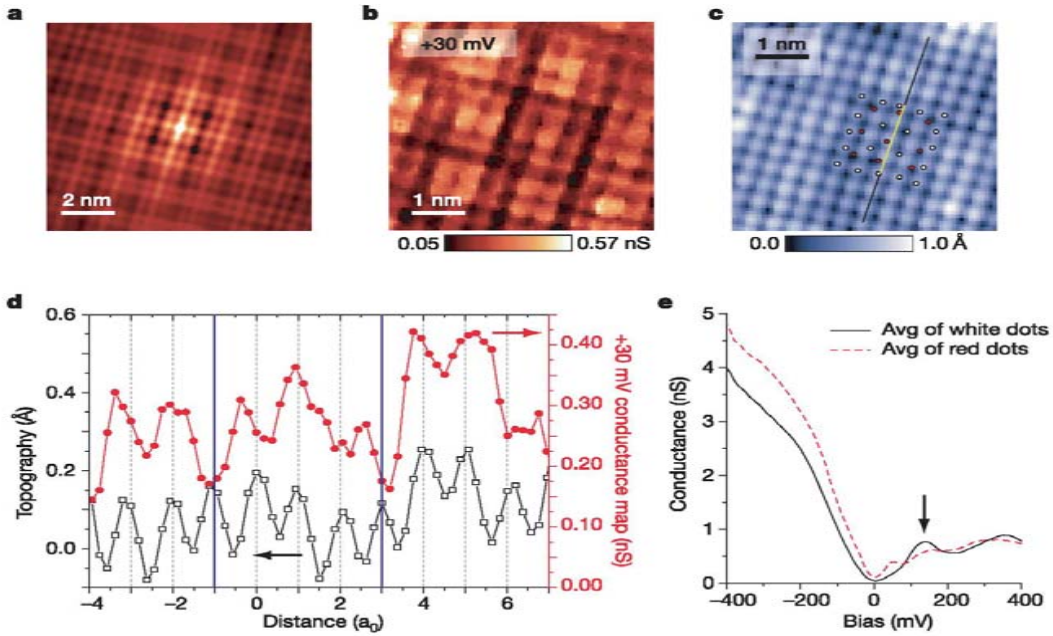

Figure 3 Electronic structure imaging within a representative $4a_0 \times 4a_0$ ‘tile’. **a**, Autocorrelation image of typical $|E| < 100$ meV LDOS maps showing the $4a_0 \times 4a_0$ structure inside a dark perimeter, which is located exactly where the 16 atoms are positioned at the common perimeter between adjacent $4a_0 \times 4a_0$ regions. **b**, A representative tile of the $4a_0 \times 4a_0$ state is seen directly. The tile exhibits a very low conductance at the perimeter and high LDOS conductance pattern with nine incommensurate maxima inside. The average spatial electronic structure in **a** is remarkably consistent with electronic structure of this (and other) tiles, but this should not be overemphasized because there is also a great deal of variability. Junction resistance for measurement was 2 GΩ at $V_s = +400$ mV. **c**, The simultaneously acquired topographic image showing the locations of what are believed to be the Cl atoms (light) above each Cu atom in the CuO_2 plane. **d**, The topographic signal (black) and simultaneously measured conductance (red) along the line shown in **c** through the tile centre. **e**, Spectra show V-shaped pseudogaps regardless of the positions. The most remarkable difference between dark (low conductance) and bright (high conductance) spots in **b** appears in the positive bias voltage. At dark spots, a strong peak is observed at $\Omega \approx +150$ meV. On average the high pseudogap (most insulating) regions exhibit a strong resonance at $\Omega \approx +150$ meV so that the $g(\mathbf{r}, E = 150\ \text{meV})$ is anticorrelated with the $g(\mathbf{r}, E)$ below 100 meV.

Hanaguri(2004)

Evidence for charge-density waves (CDWs) in cuprates

$Ca_{2-x}Na_xCuO_2Cl_2$

(STM)

Checkerboard

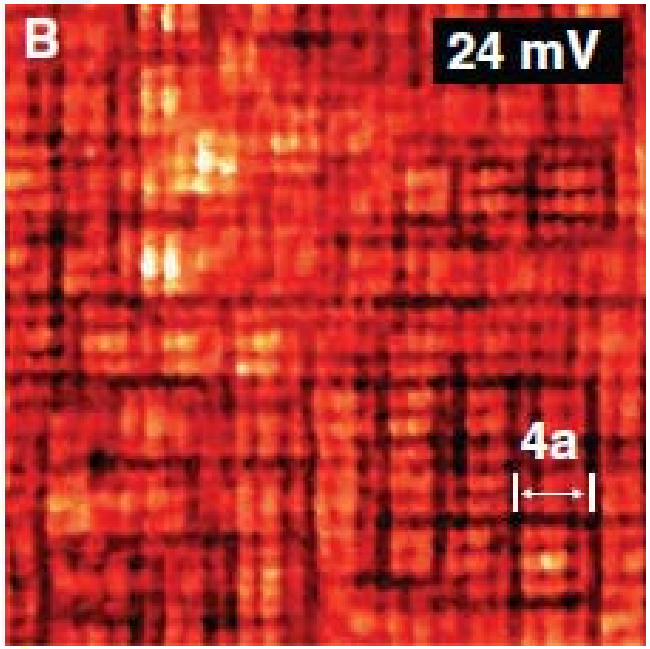

Bi-based ceramics (STM)

one-dimensional modulation

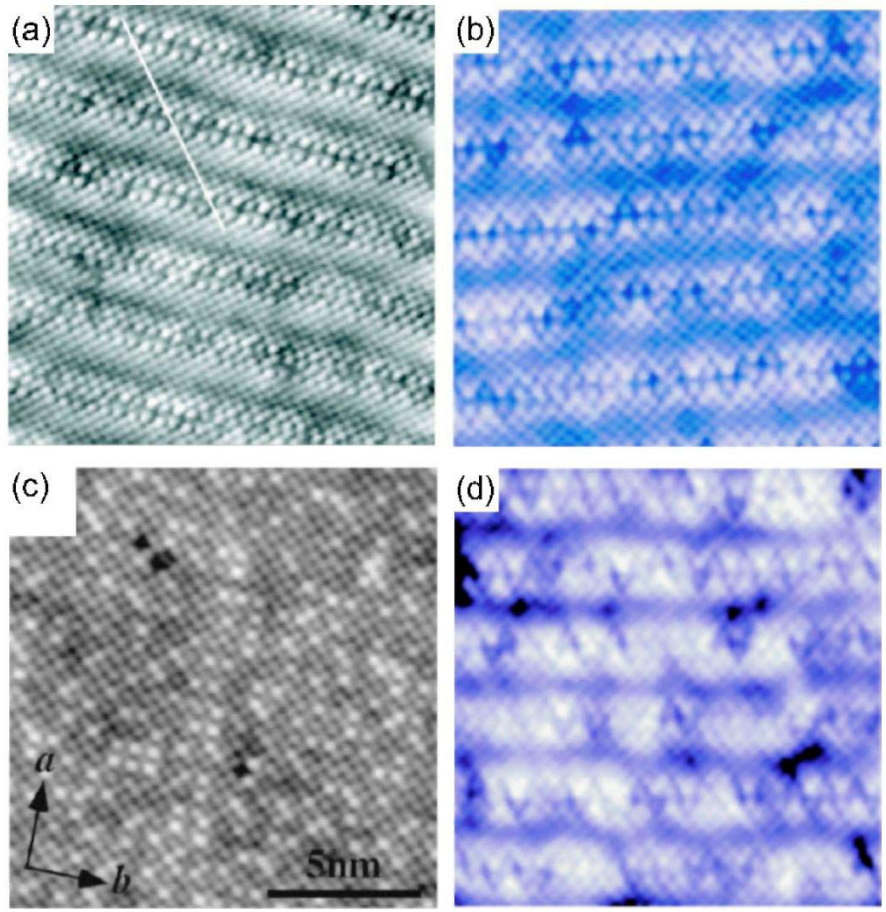

Inherent nanoscale inhomogeneity of measured energy gaps and local critical temperatures ($Bi_2Sr_2CaCu_2O_{8+\delta}$)

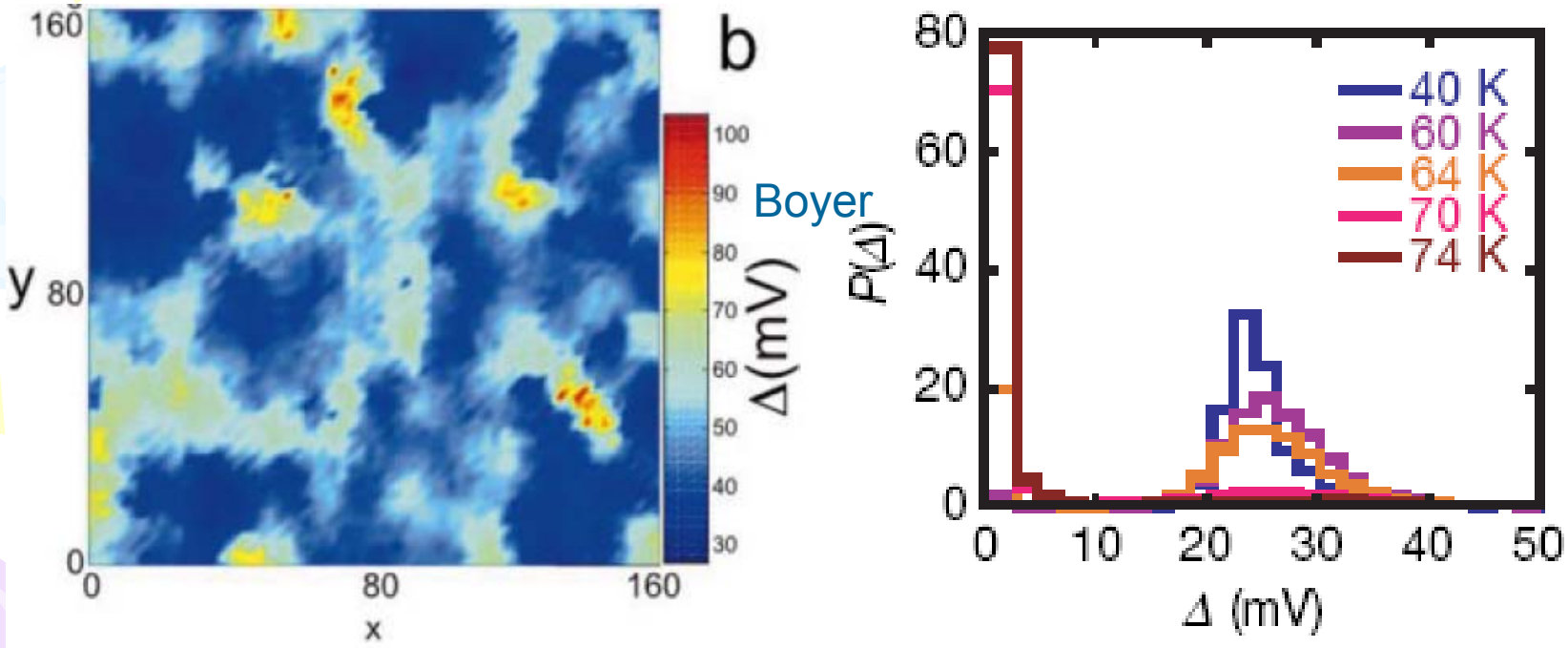

Superconducting gaps are homogeneous, CDW gaps (pseudogaps) vary strongly: Boyer et al. (2007)

CONVENTIONAL *S*- AND *D*- SUPERCONDUCTING PAIRING

Two-dimensional diagram of the order parameter/gap Δ

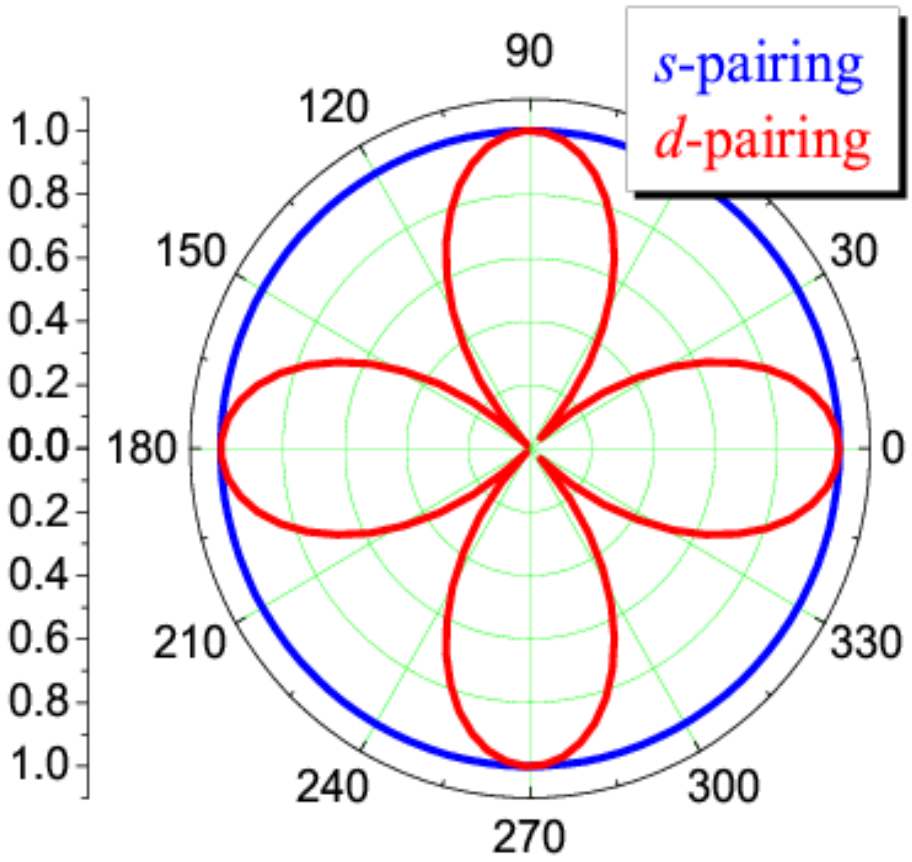

FERMI SURFACE MAPS OF THE DIELECTRIC Σ AND SUPERCONDUCTING Δ ORDER PARAMETERS

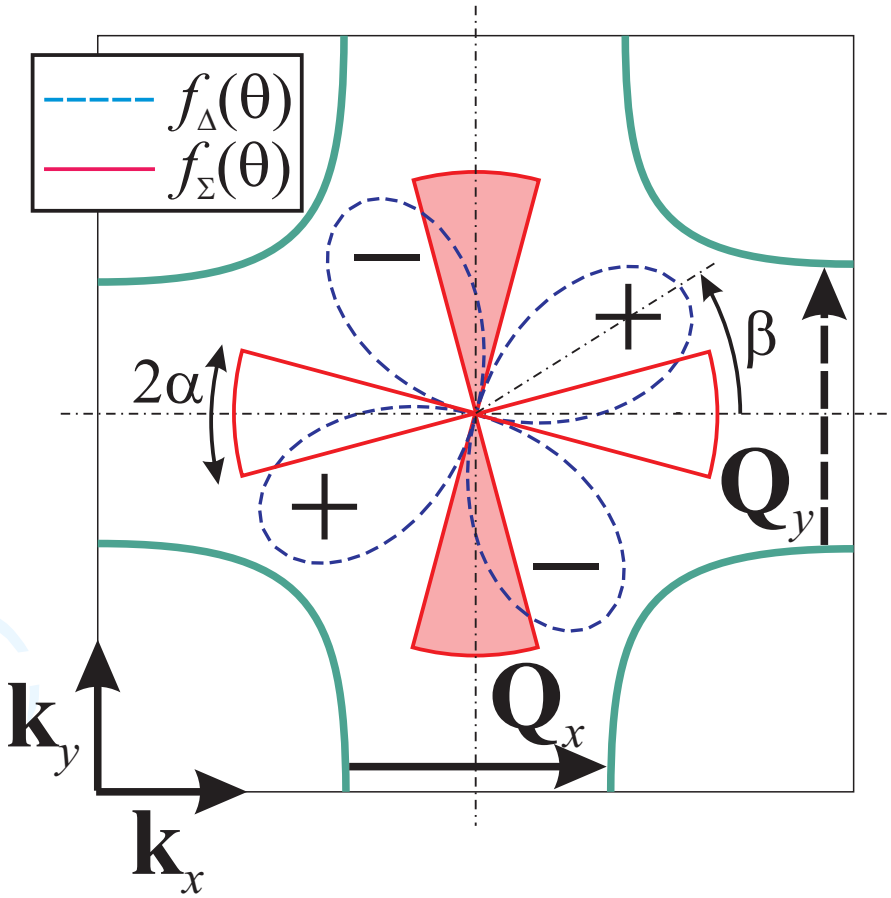

S- and *d*- conventional superconducting pairing

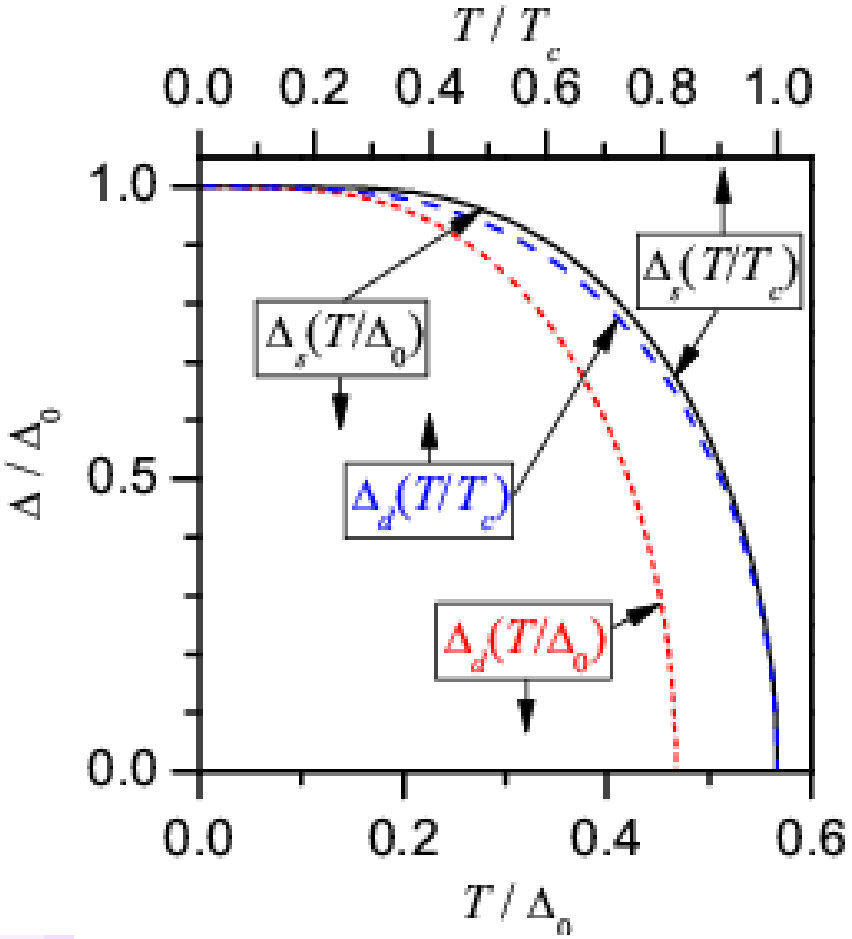

S

$$\frac{\Delta_0}{T_c} \approx 1.76$$

$$\frac{T_c}{\Delta_0} \approx 0.57$$

D

$$\frac{\Delta_0}{T_c} \approx 2.12$$

$$\frac{T_c}{\Delta_0} \approx 0.47$$

THEORETICAL DESCRIPTION

System of equations for order parameters

$$\int_{\beta-\alpha}^{\beta+\alpha} I_M(\sqrt{\Sigma^2+\Delta^2\cos^2 2\theta}, k_BT, \Sigma_0)d\theta = 0$$

$$\int_{\beta-\alpha}^{\beta+\alpha} I_M(\sqrt{\Sigma^2+\Delta^2\cos^2 2\theta}, k_BT, \Delta_0\cos 2\theta)\cos^2 2\theta d\theta + \int_{\beta+\alpha}^{\Omega+\beta-\alpha} I_M(\Delta\cos 2\theta, k_BT, \Delta_0\cos 2\theta)\cos^2 2\theta d\theta = 0$$

In the adopted order parameter configuration

$\mu\Omega = 2\alpha$;

$\Omega = \pi/2$ and π for the checkerboard and unidirectional CDW patterns, respectively; μ = is the dielectrically gapped portion of Fermi surface

Mühlschlegel integral:

$$I_M(X,T,X_0) = \int_0^\infty d\xi\left(\frac{1}{\sqrt{\xi^2+X^2}}\tanh\frac{\sqrt{\xi^2+X^2}}{2T} - \frac{1}{\sqrt{\xi^2+X_0^2}}\right)$$

Δ_0 and Σ_0 are the bare superconducting and CDW order parameters, respectively

$\sigma_0 = \Sigma_0/\Delta_0$

Phase diagrams

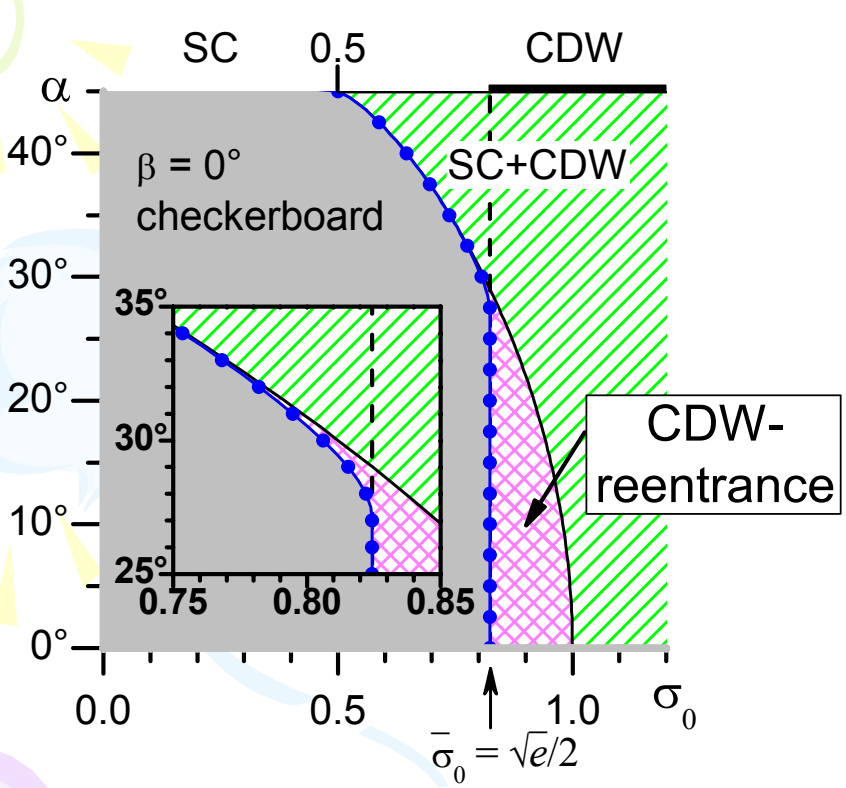

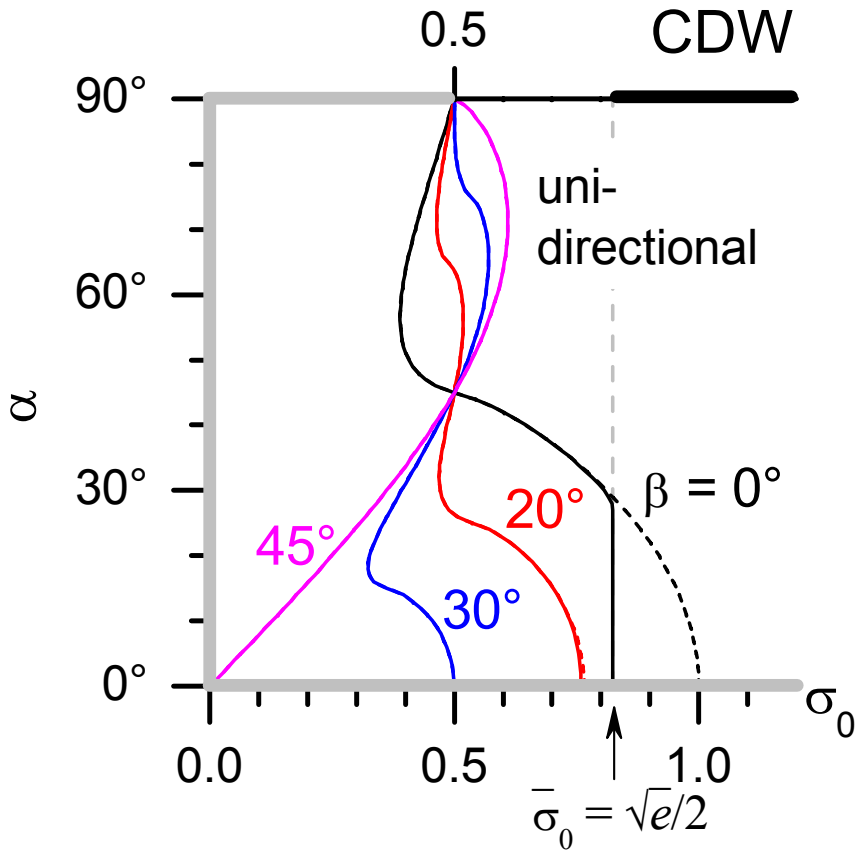

Order parameters

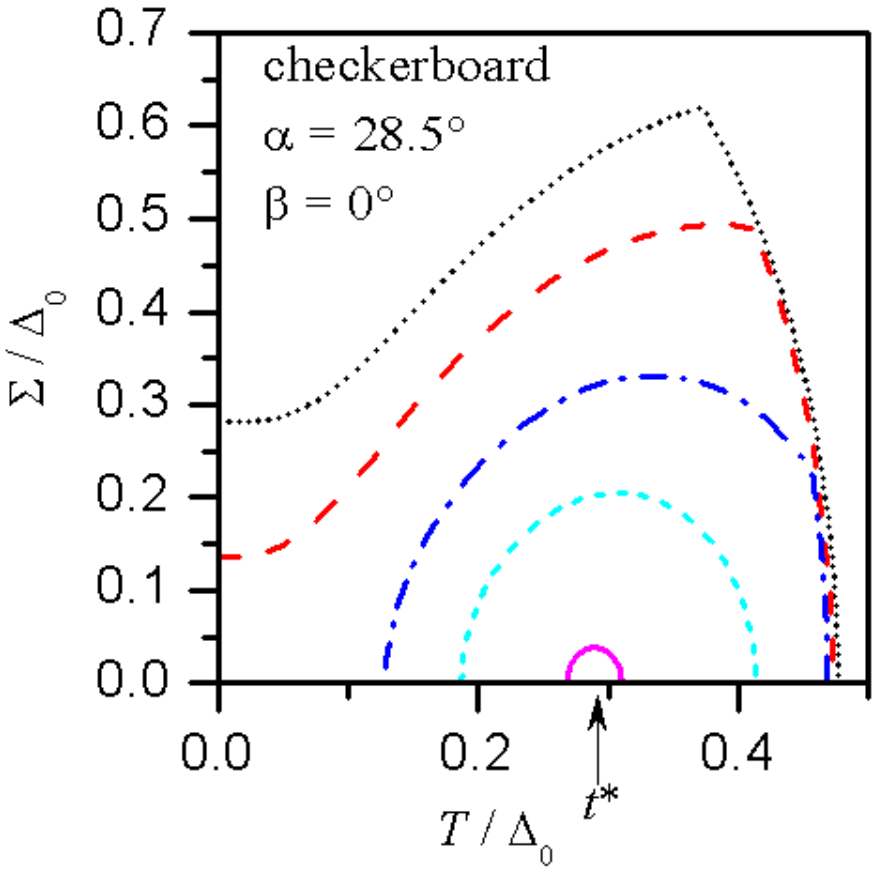

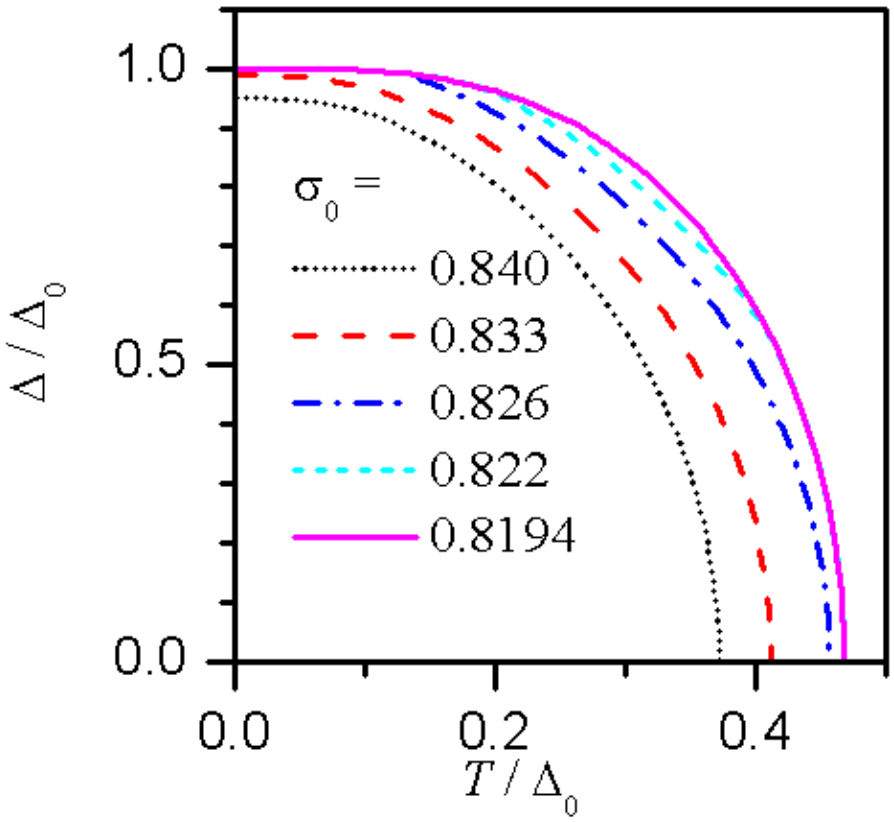

Gap roses and gap bands

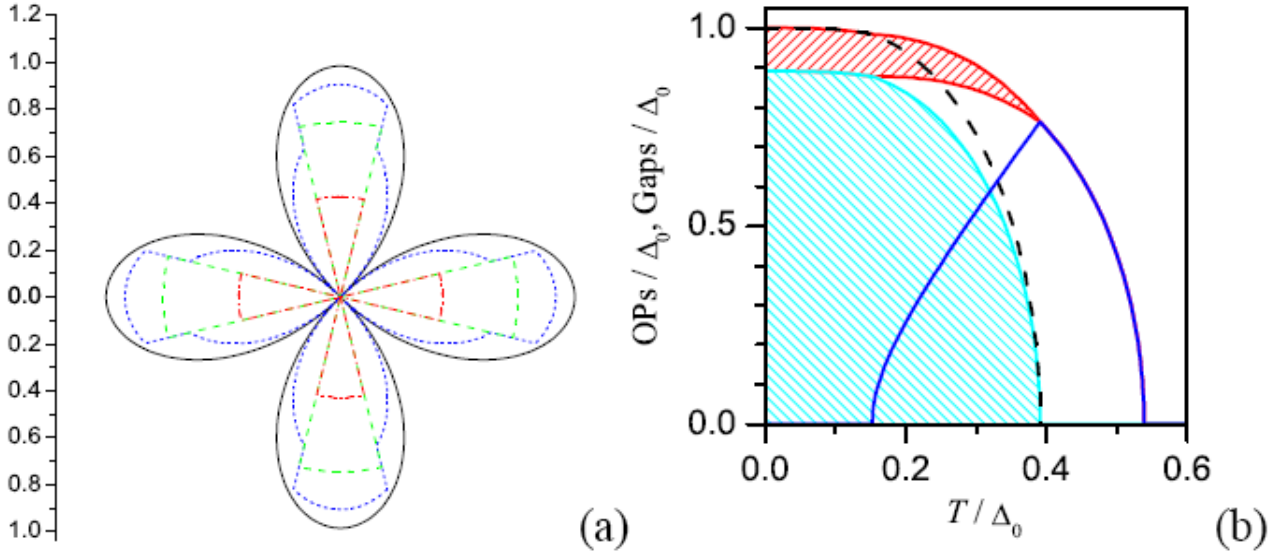

(a) "Gap rose" in the momentum space at normalized temperatures $t = 0.15$ (solid), 0.3 (short-dashed), 0.4 (long-dashed), 0.5 (dash-dotted curve). (b) T-dependences of CDW (solid curve) and SC (dashed curve) order parameters and gap bands (obtained at the angular scanning in the momentum space) on dielectrized (right hatch) and non-dielectrized (left hatch) Fermi surface (FS) sections. In both panels $\mu = 0.3$, $\beta = 0°$, anf $\sigma_0 = 0.95$.

Gap roses

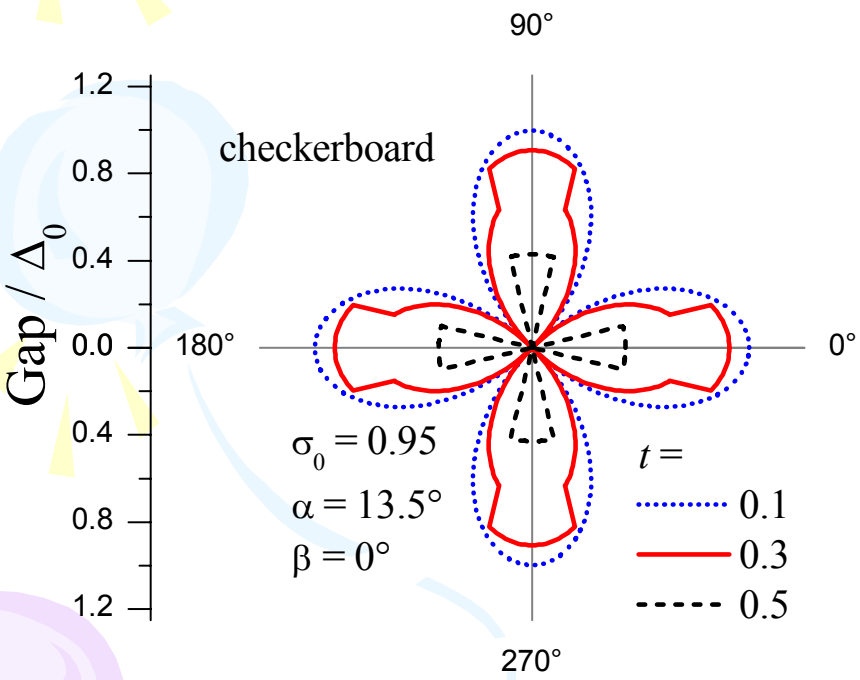
90°
180°
0°
270°
1.2
0.8
0.4
0.0
0.4
0.8
1.2
Gap / Δ0
checkerboard
σ0 = 0.95
α = 13.5°
β = 0°
t =
0.1
0.3
0.5

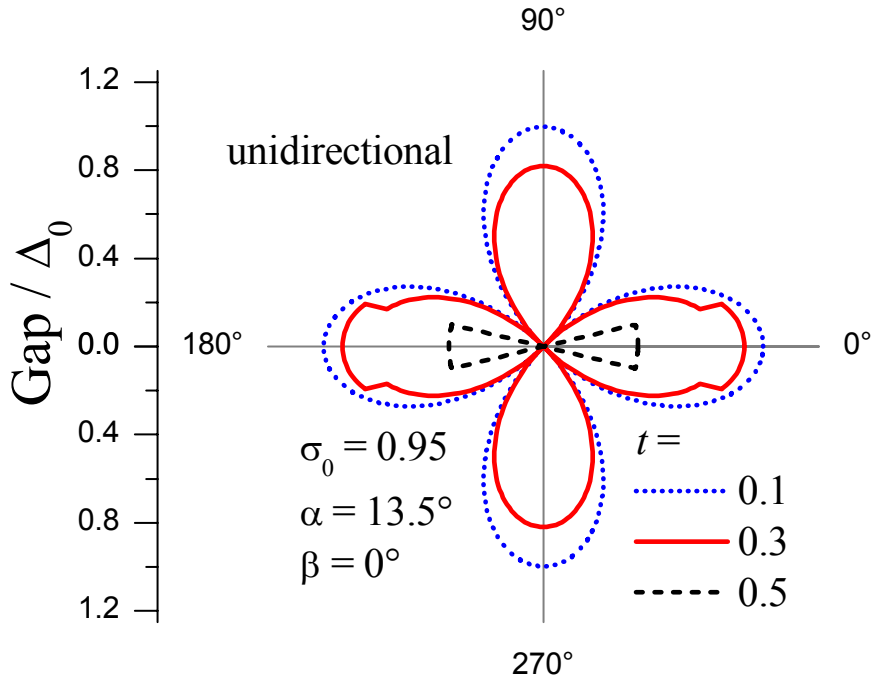
90°
180°
0°
270°
1.2
0.8
0.4
0.0
0.4
0.8
1.2
Gap / Δ0
unidirectional
σ0 = 0.95
α = 13.5°
β = 0°
t =
0.1
0.3
0.5

Complete dielectric gapping

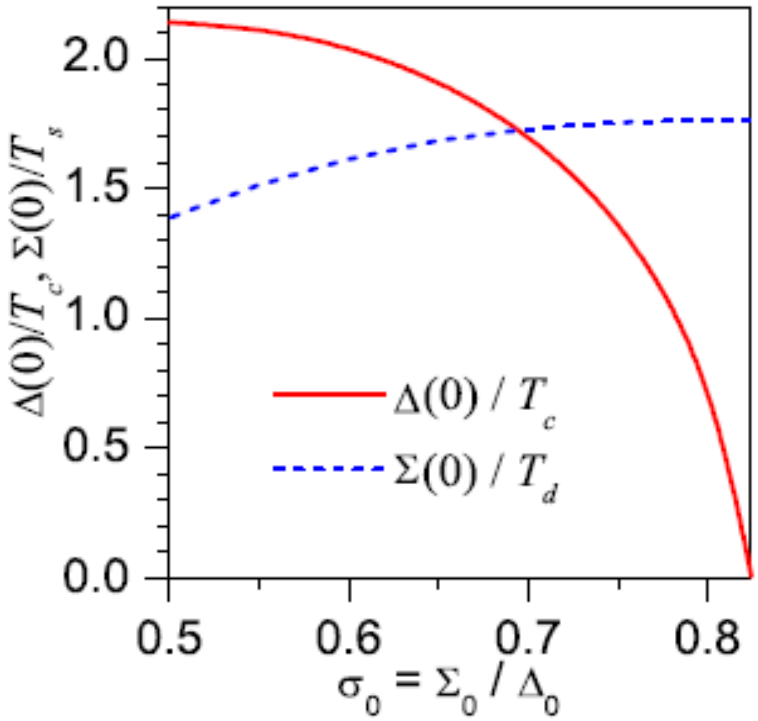

σ_0-dependences of the ratios between the order parameters at $T = 0$ and the relevant critical temperatures for complete CDW gapping.

One more puzzle

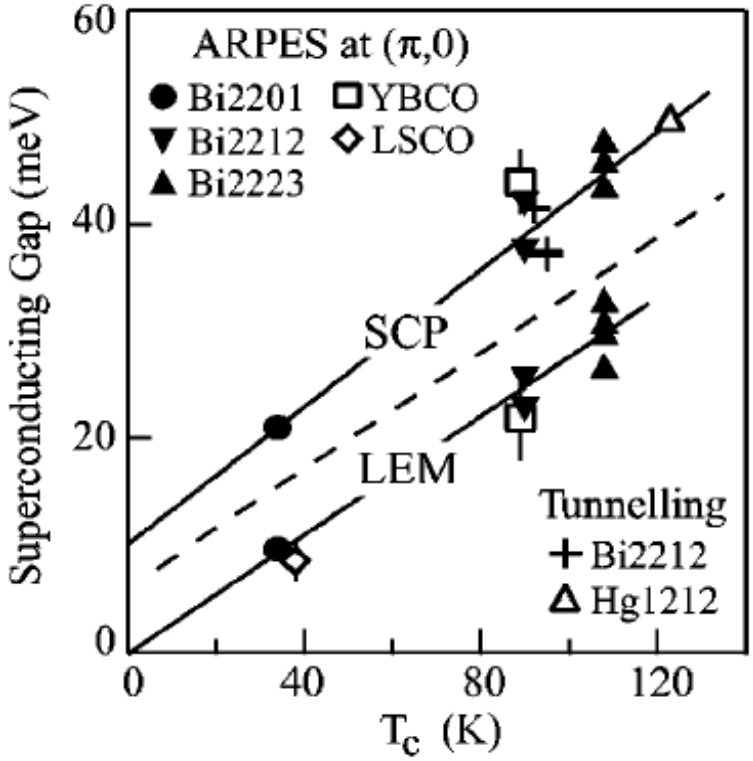

FIG. 50. Superconducting gap magnitude estimated from the superconducting peak position and the leading-edge midpoint shift (separated by the dashed line), plotted vs T_c for various optimally doped materials. From Feng, Damascelli, *et al.*, 2002.

The ratio $2\Delta(0)/T_c \approx 5.5$

The ratio $R = \Delta(0)/T_c$

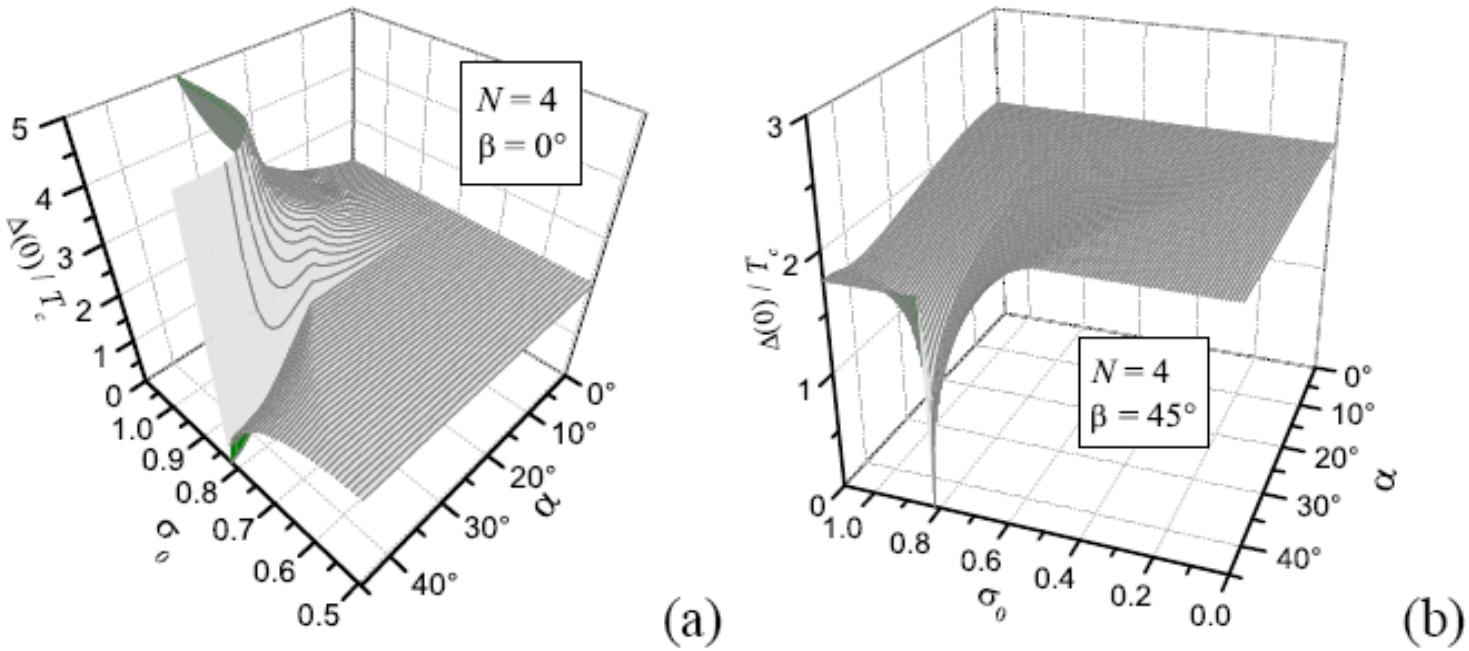

3D-plots of the ratio $R = \Delta(0)/T_c$ on the phase plane $\alpha - \sigma_0$ for CDW (a) $d_{x^2-y^2}$- and (b) d_{xy}-wave superconductors in the checkerboard CDW configuration.

$\Delta(0)/T_c$

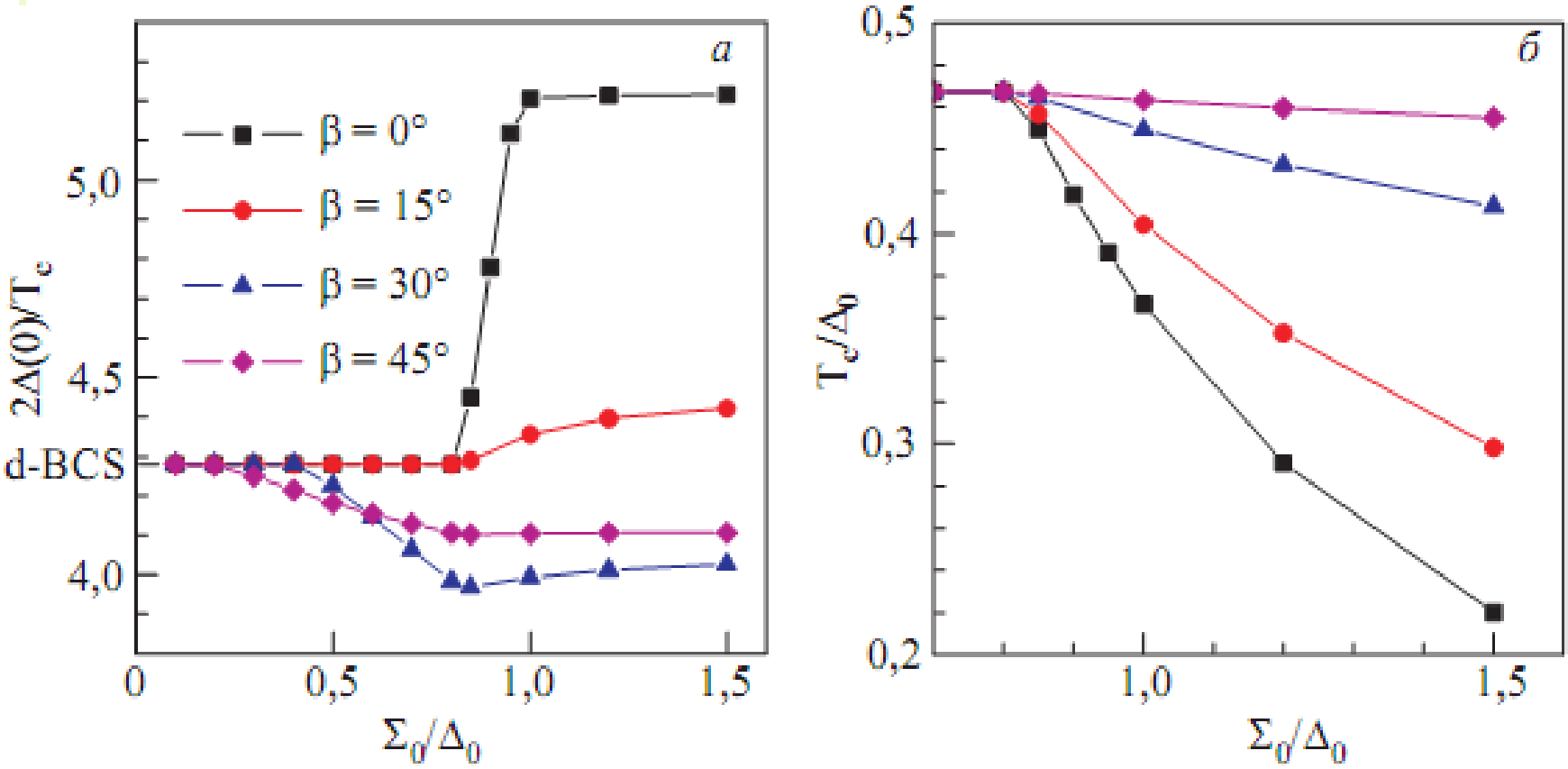

checkerboard, μ = 0.3

dc Josephson current. Geometry of the junction

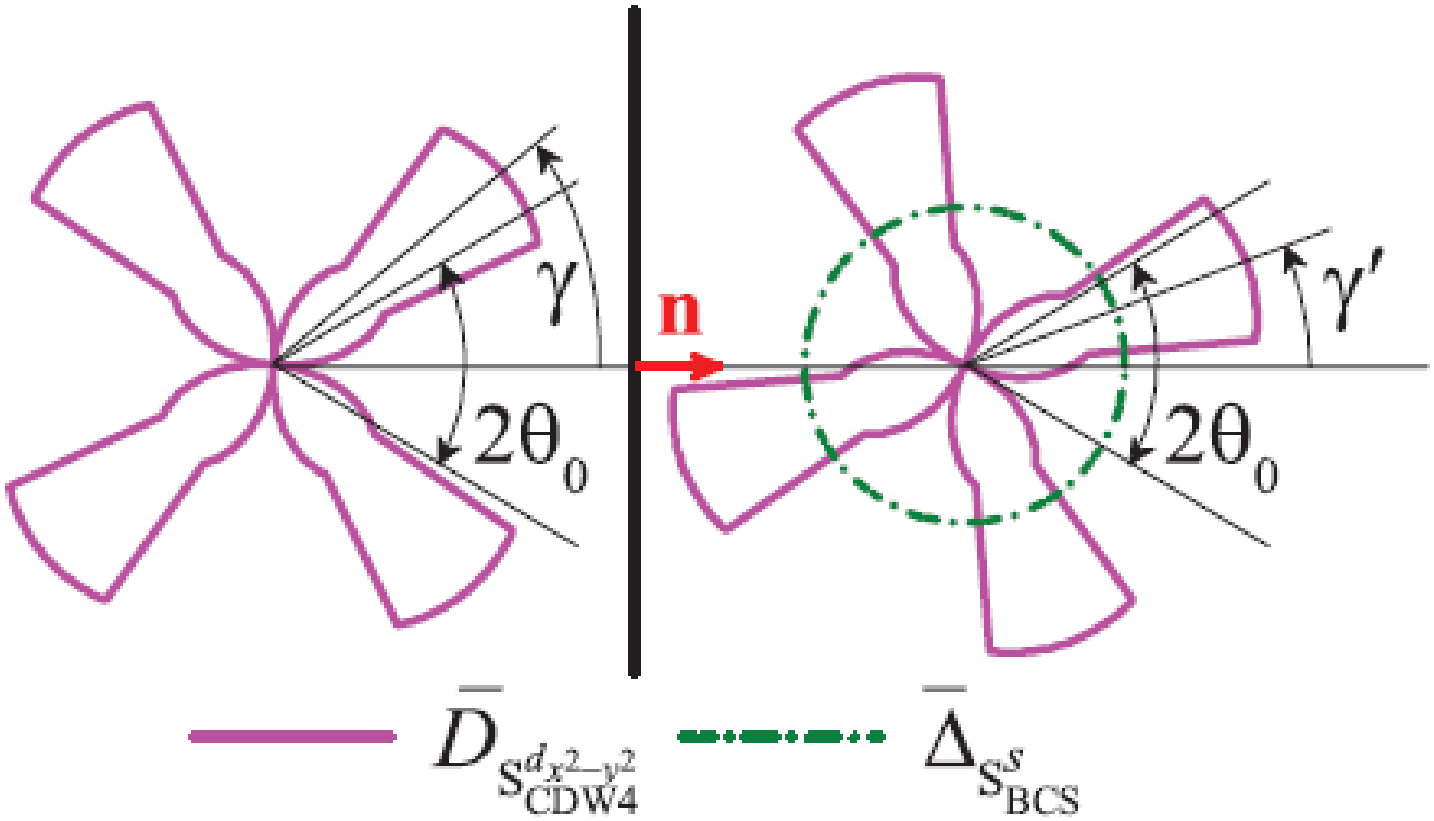

Directional tunneling for an example of non-symmetric junctions

The weight factor $w(\theta)$

$$w(\theta) = \exp\left[-\ln 2 \times \left(\frac{\tan\theta}{\tan\theta_0}\right)^2\right]$$

$$I_c(T) = \frac{\Delta(0)\Delta^*(0)}{2eR_N} i_c(T),$$

$$i_c(T) = \frac{1}{2\pi}\int_{\theta_d} w(\theta)\cos[2(\theta-\gamma)]\, P\left[\Delta^*(T), \sqrt{\Sigma^2 + \Delta^2(T)\cos^2[2(\theta-\gamma)]}\right] d\theta$$
$$+ \frac{1}{2\pi}\int_{\theta_{nd}} w(\theta)\cos[2(\theta-\gamma)]\, P[\Delta^*(T), |\Delta(T)\cos 2(\theta-\gamma)|]\, d\theta.$$

$$P(\Delta_1, \Delta_2) = \int_{\min\{\Delta_1,\Delta_2\}}^{\max\{\Delta_1,\Delta_2\}} \frac{dx \tanh\frac{x}{2T}}{\sqrt{(x^2-\Delta_1^2)(\Delta_2^2-x^2)}}.$$

Parameter dependences of current amplitudes

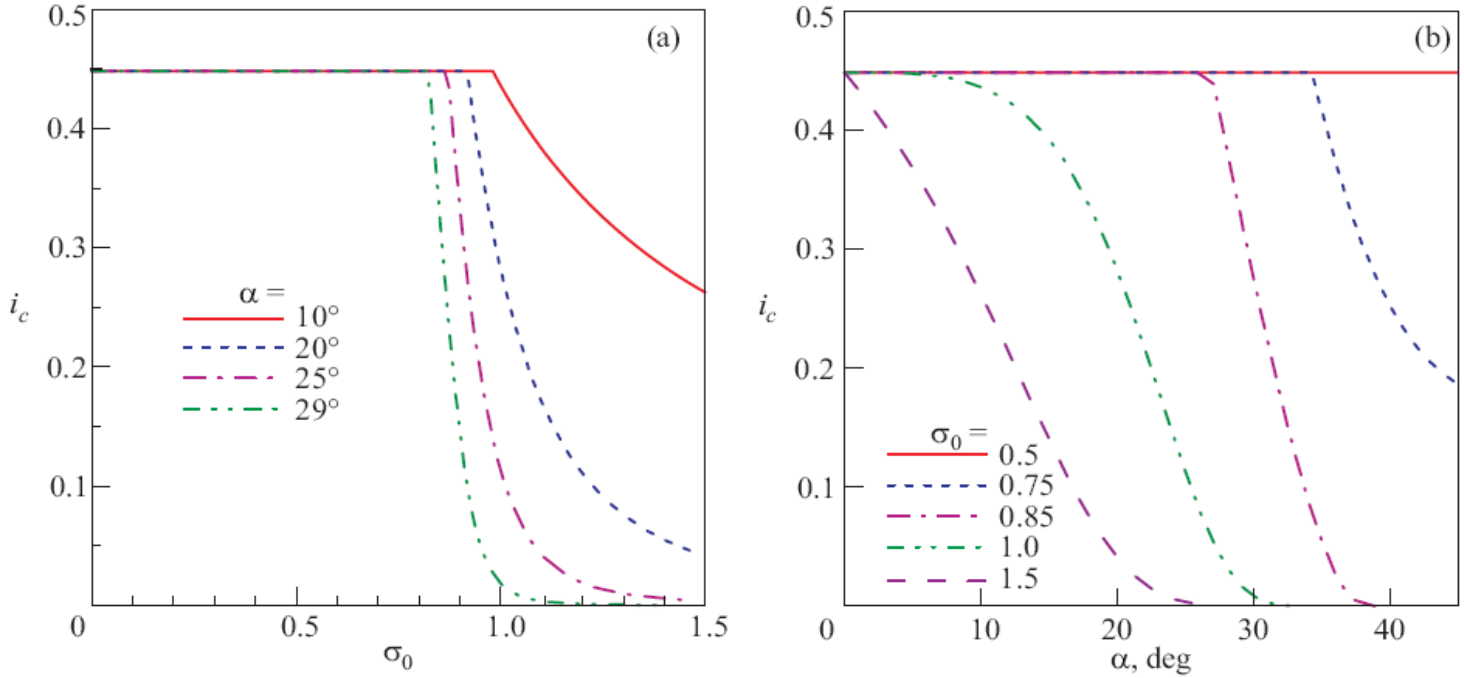

$$S^{d_{x^2-y^2}}_{CDW4} - I - S^{d_{x^2-y^2}}_{CDW4} \quad \text{junction with} \quad \gamma = \gamma' = 0$$

Parameter dependences of current amplitudes

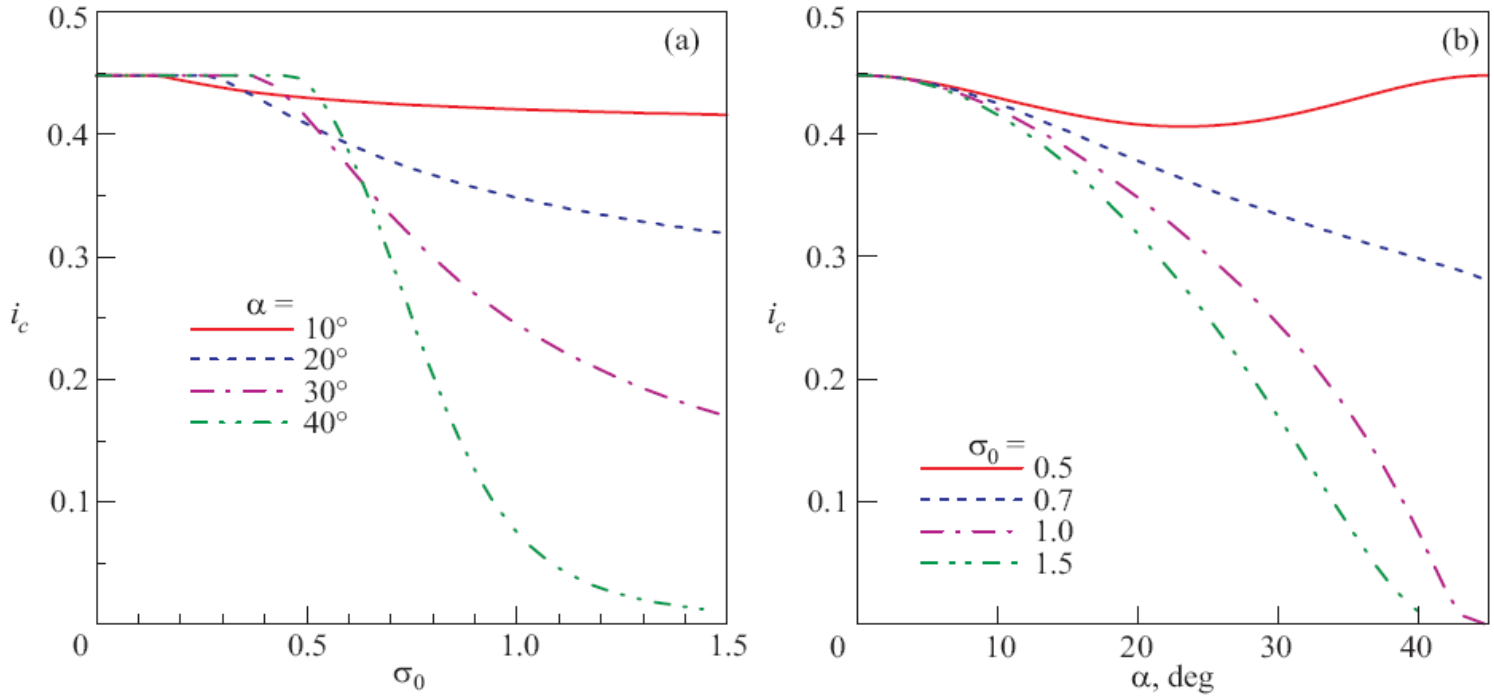

symmetrical $S^{d_{xy}}_{CDW4} - I - S^{d_{xy}}_{CDW4}$ junction

Parameter dependences of current amplitudes

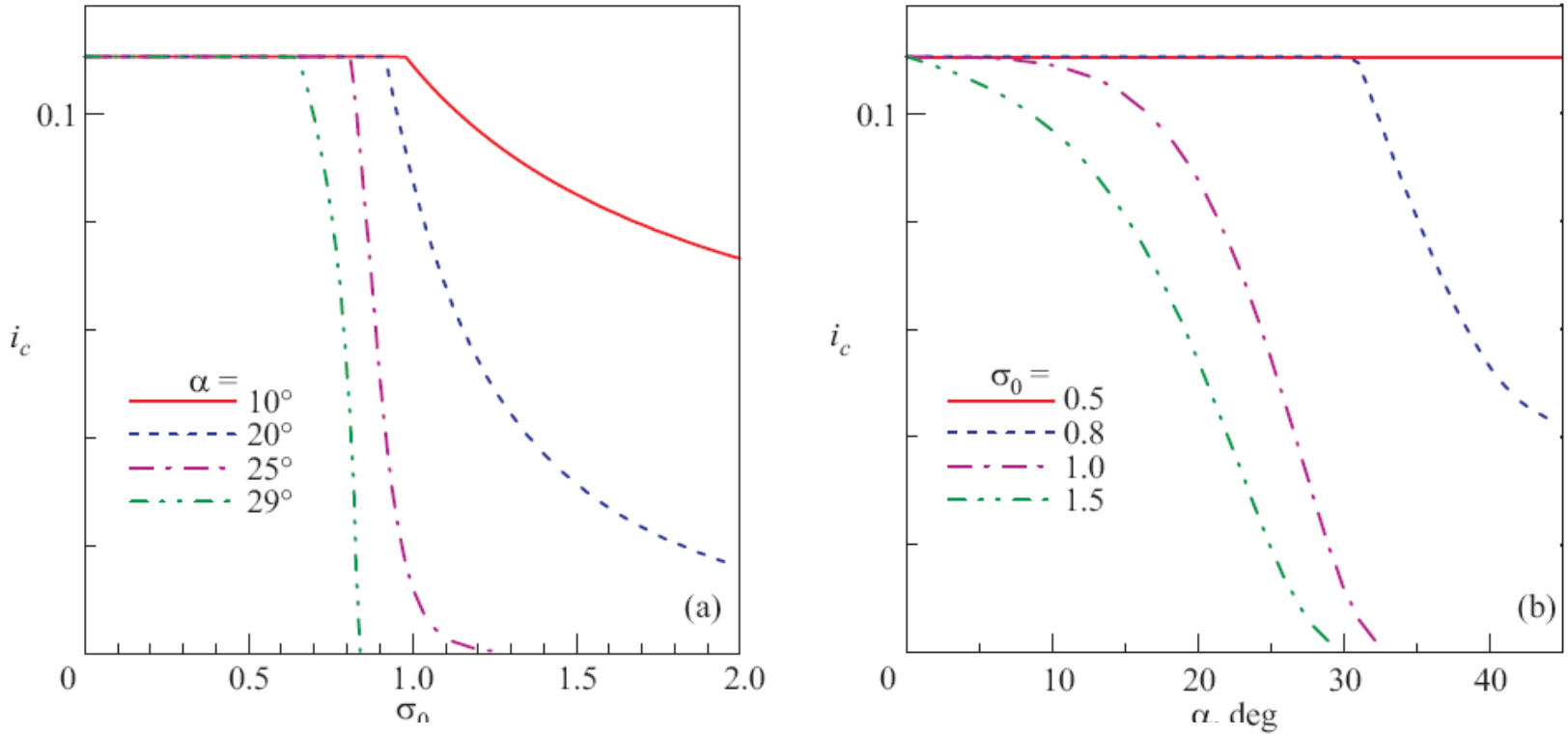

nonsymmetrical $S^{d_{x^2-y^2}}_{CDW4} - I - S^{s}_{BCS}$ junction

$\delta_{BCS} = 0.1$

$\delta_{BCS} = \Delta_{BCS}(T=0)/\Delta_0$

Parameter dependences of current amplitudes in the reentrance region

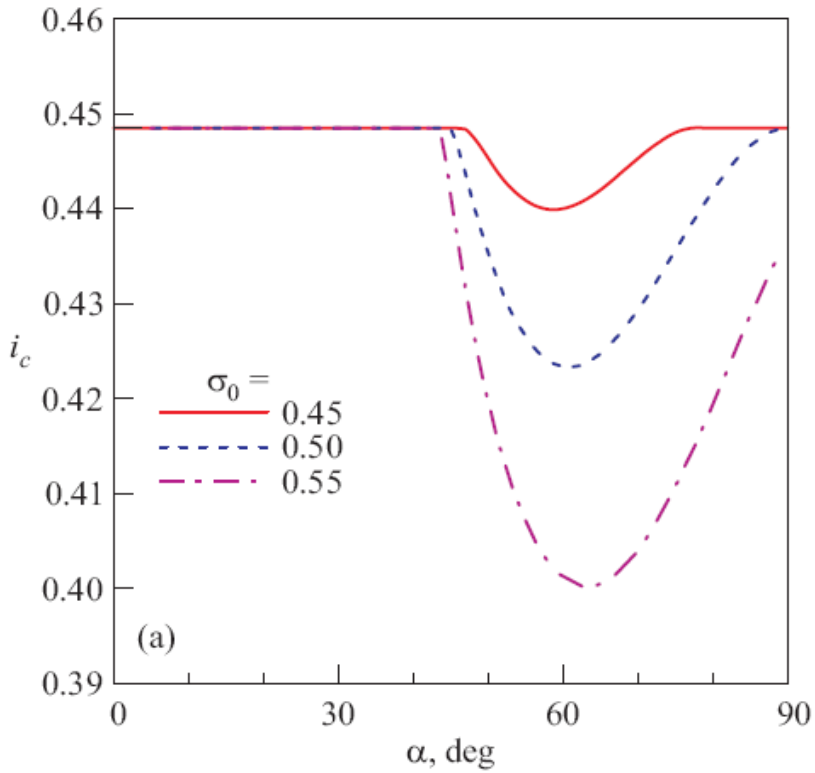

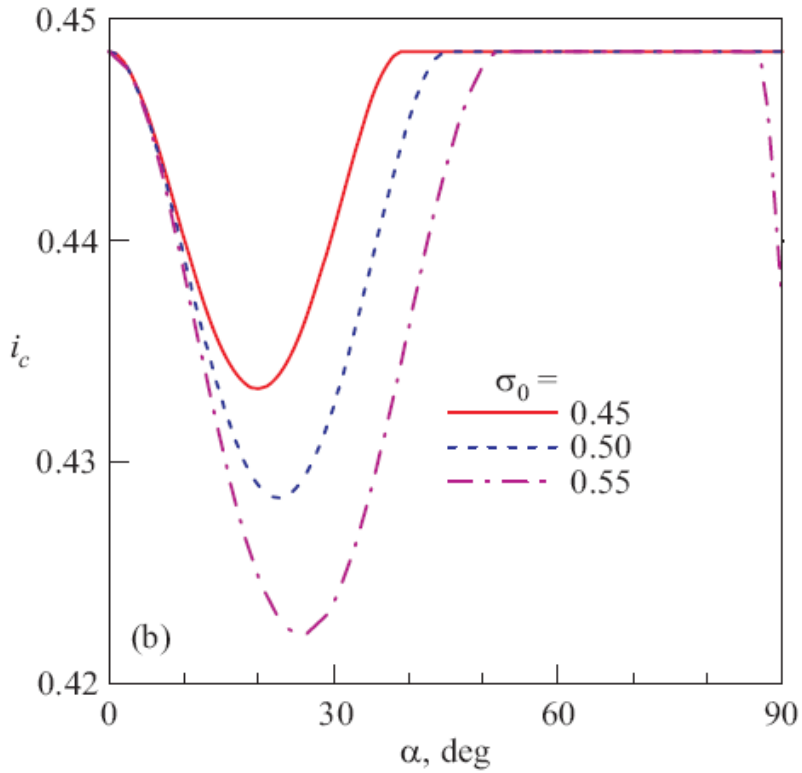

(a) $S^{d_{x^2-y^2}}_{CDW2} - I - S^{d_{x^2-y^2}}_{CDW2}$ and (b) $S^{d_{xy}}_{CDW2} - I - S^{d_{xy}}_{CDW2}$

Parameter dependences of current amplitudes in the reentrance region

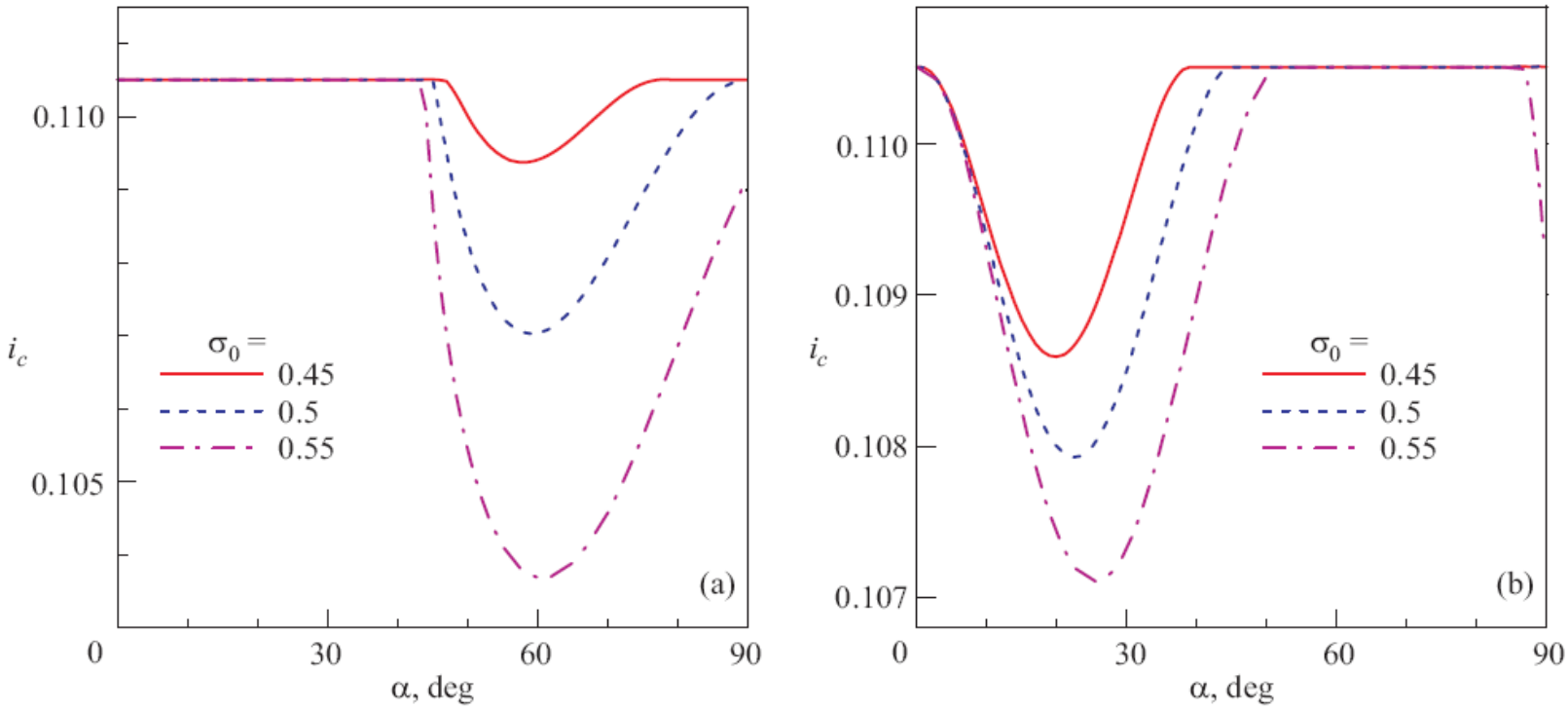

non-symmetrical $S^{d_{x^2-y^2}}_{CDW2} - I - S^{s}_{BCS}$ (a) and $S^{d_{xy}}_{CDW2} - I - S^{s}_{BCS}$ (b) junctions

Influence on the directional tunneling angle θ_0

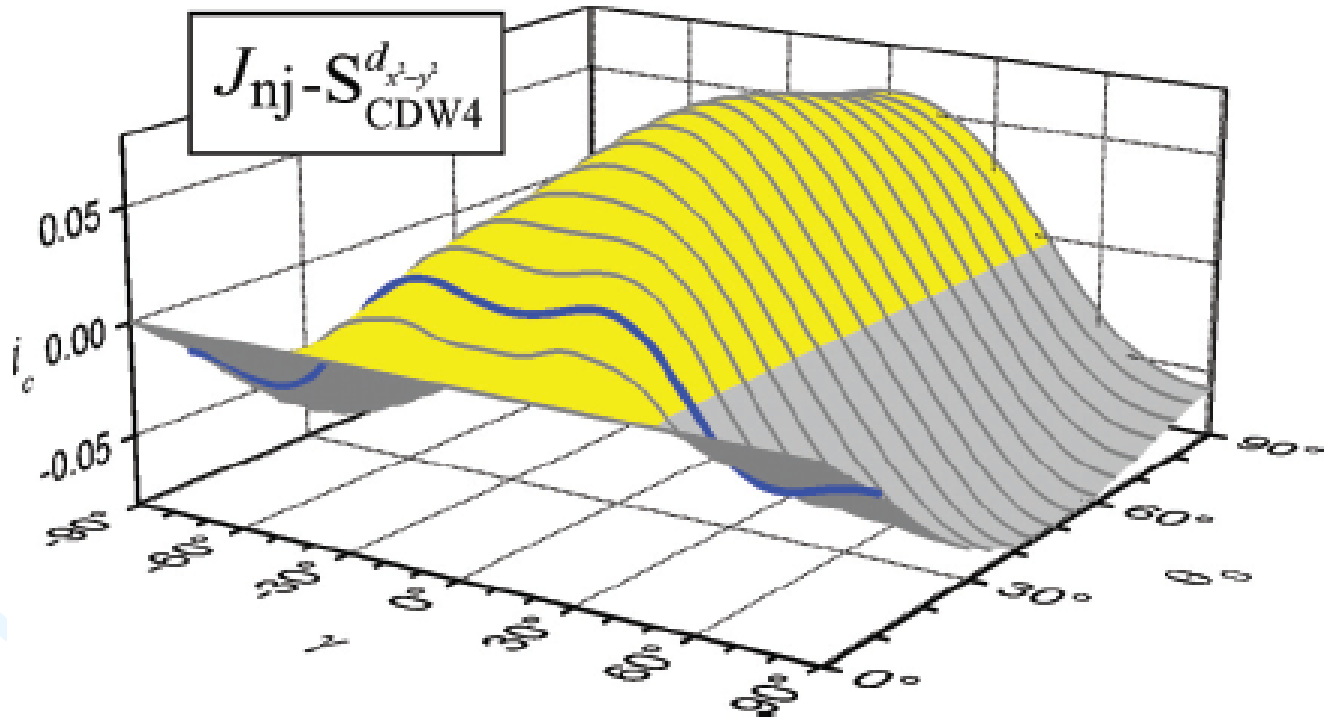

Angular current dependences for symmetric d-wave superconducting junctions with (a) and without (b) checkerboard CDWs

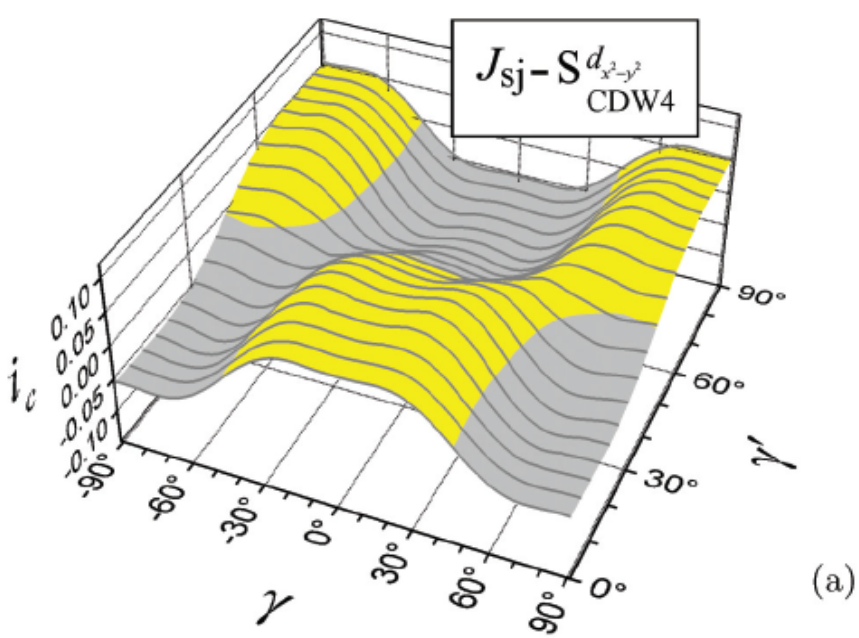

(a)

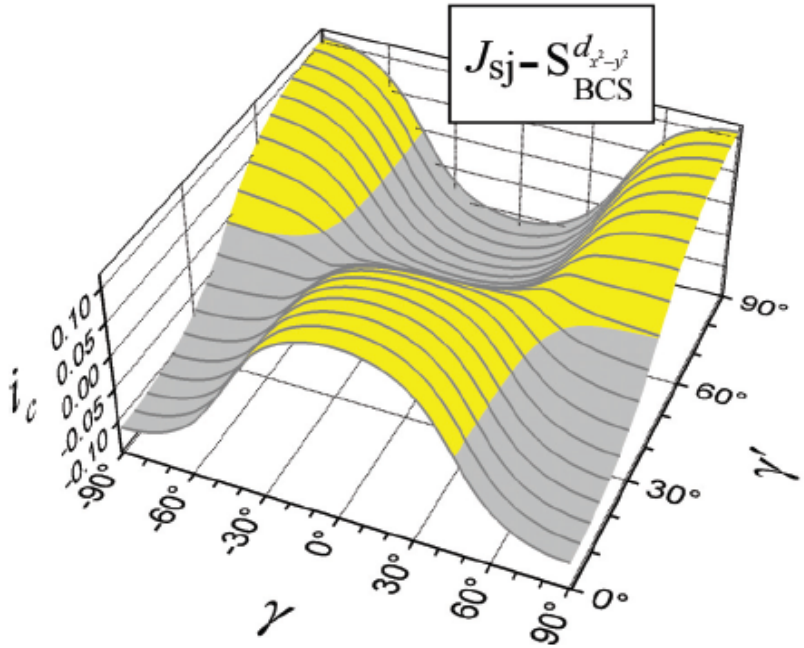

(b)

Angular current dependences for symmetric d-wave superconducting junctions with unidirectional CDWs

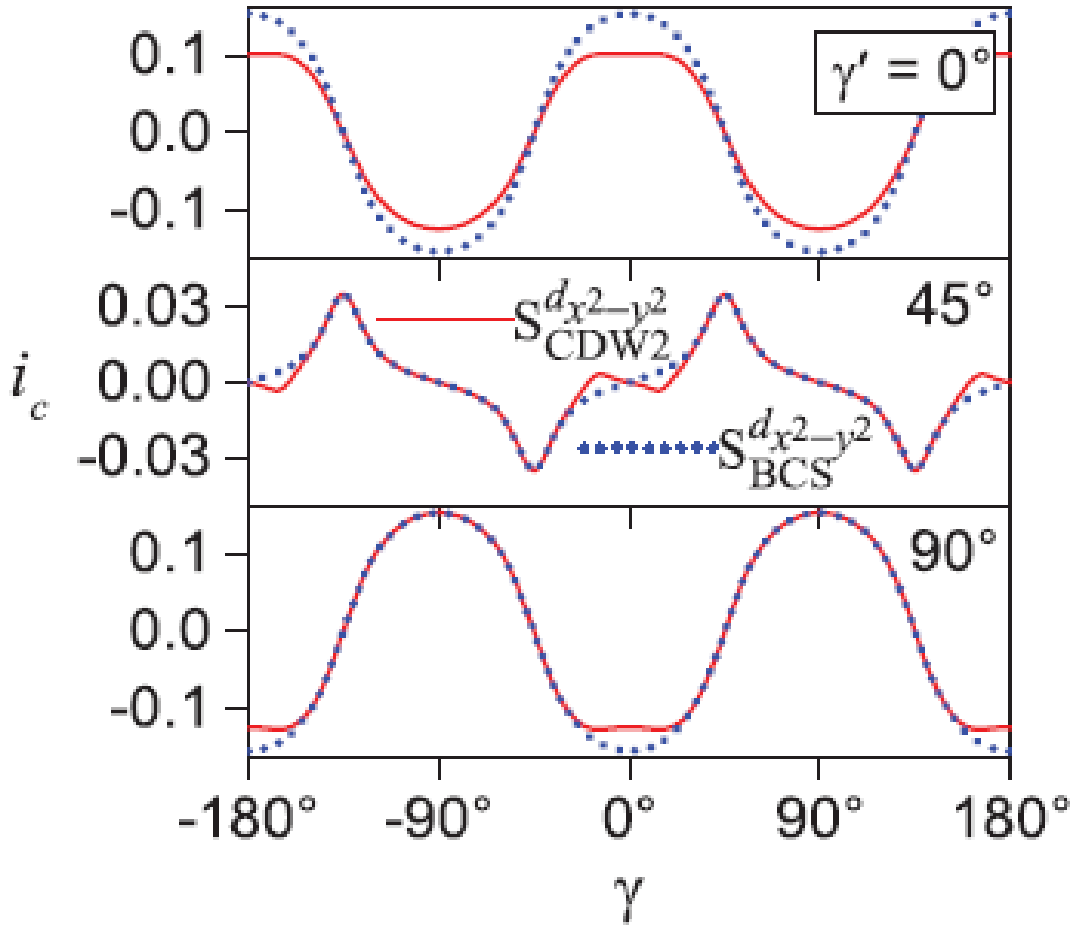

Angular current dependences for symmetric d-wave superconducting junctions with correlated rotations of checkerboard (a) and unidirectional (b) CDWs

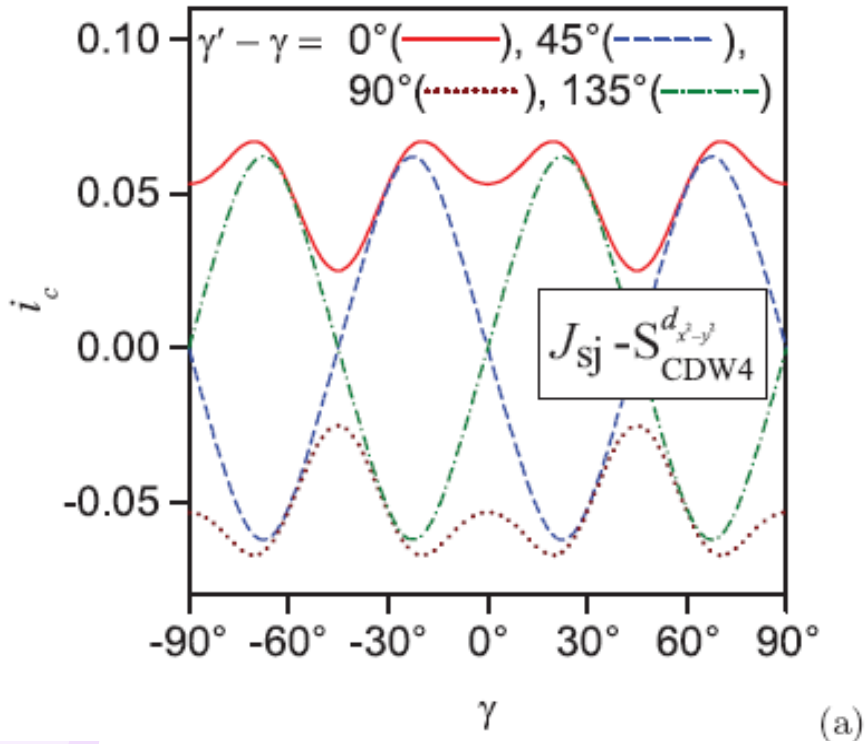

(a)

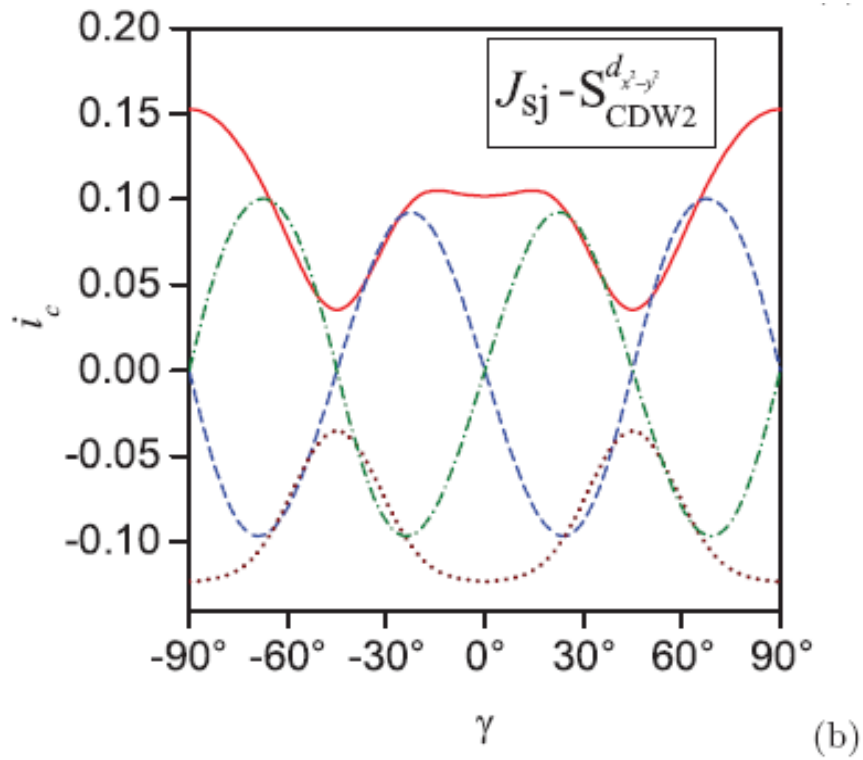

(b)

Angular current dependences for symmetric CDW superconducting junctions with different symmetries of the superconducting order parameter and checkerboard CDW configuration

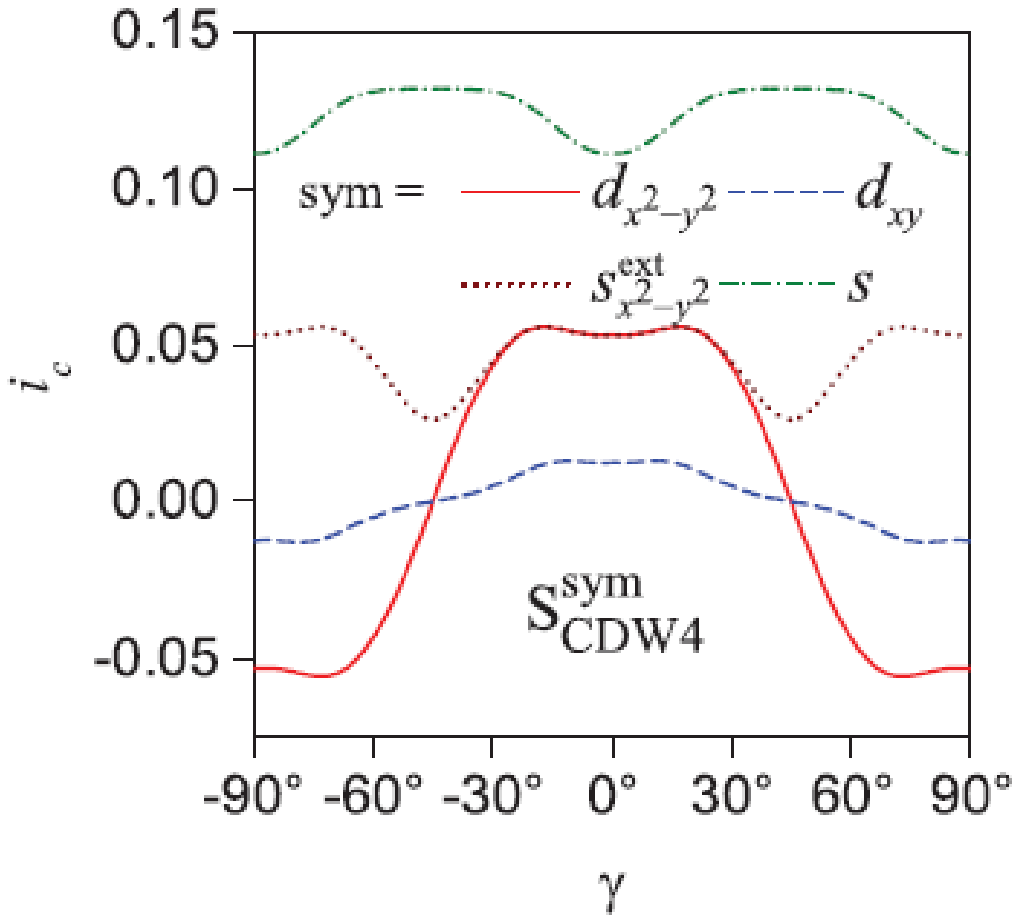

Angular current dependences for non-symmetric CDW superconducting junctions with different symmetries of the superconducting order parameter and checkerboard (a) and unidirectional (b) CDW configurations

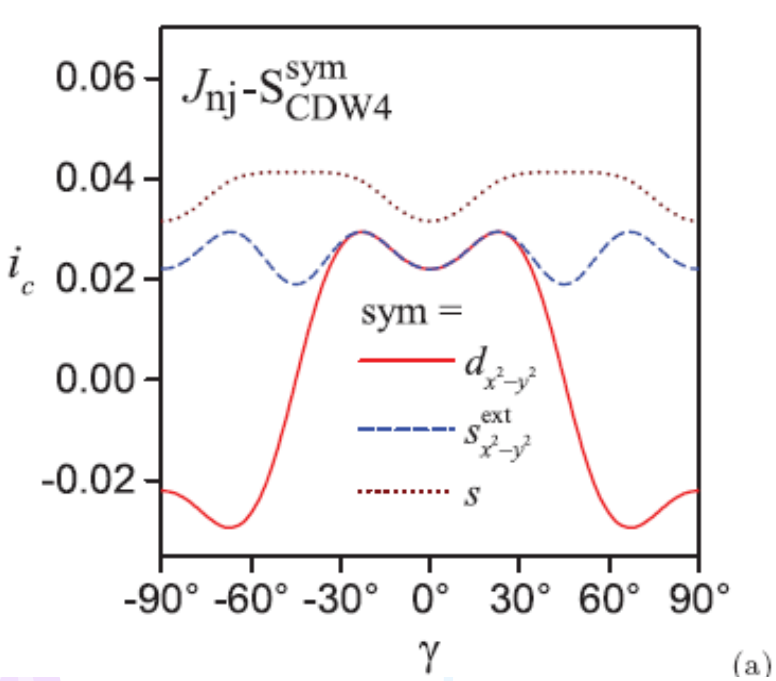

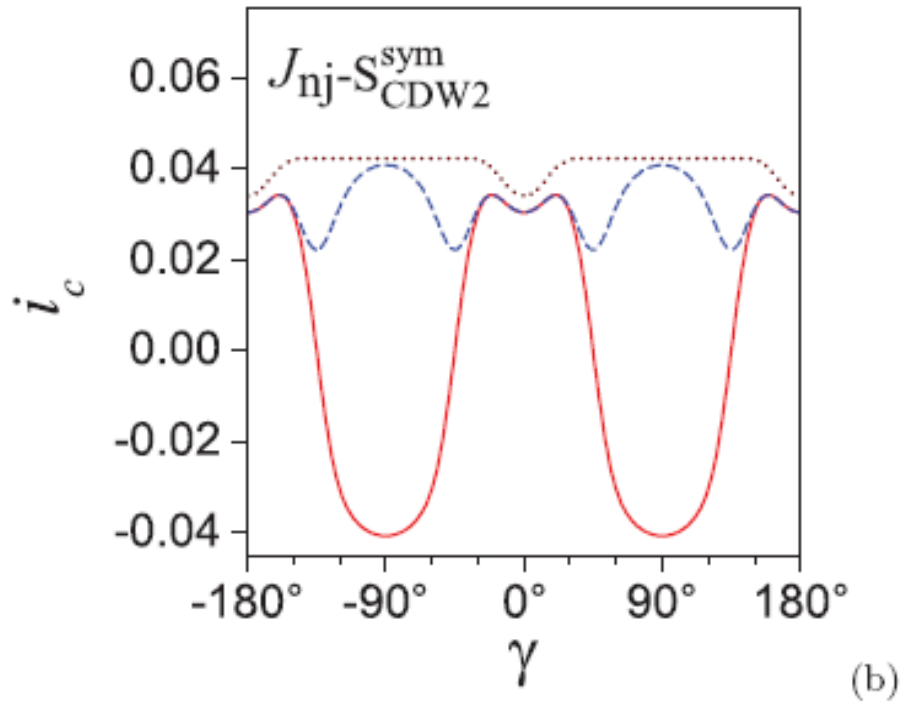

Proportionality between Josephson current and product of superconducting gaps: symmetric junctions involving d- and s-wave superconductors ($\tau = T/T_c$ as a driving force)

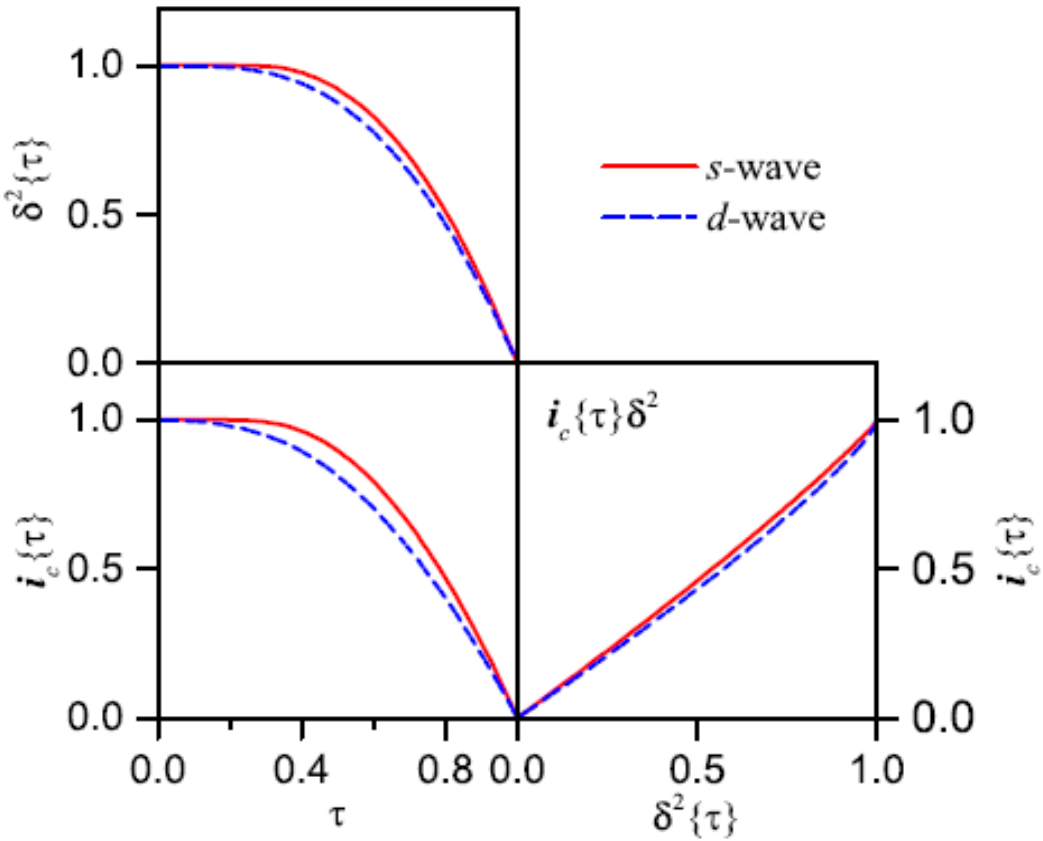

Proportionality between Josephson current and product of superconducting gaps: symmetric junctions involving d-wave superconductors with unidirectional CDWs (α as a driving force)

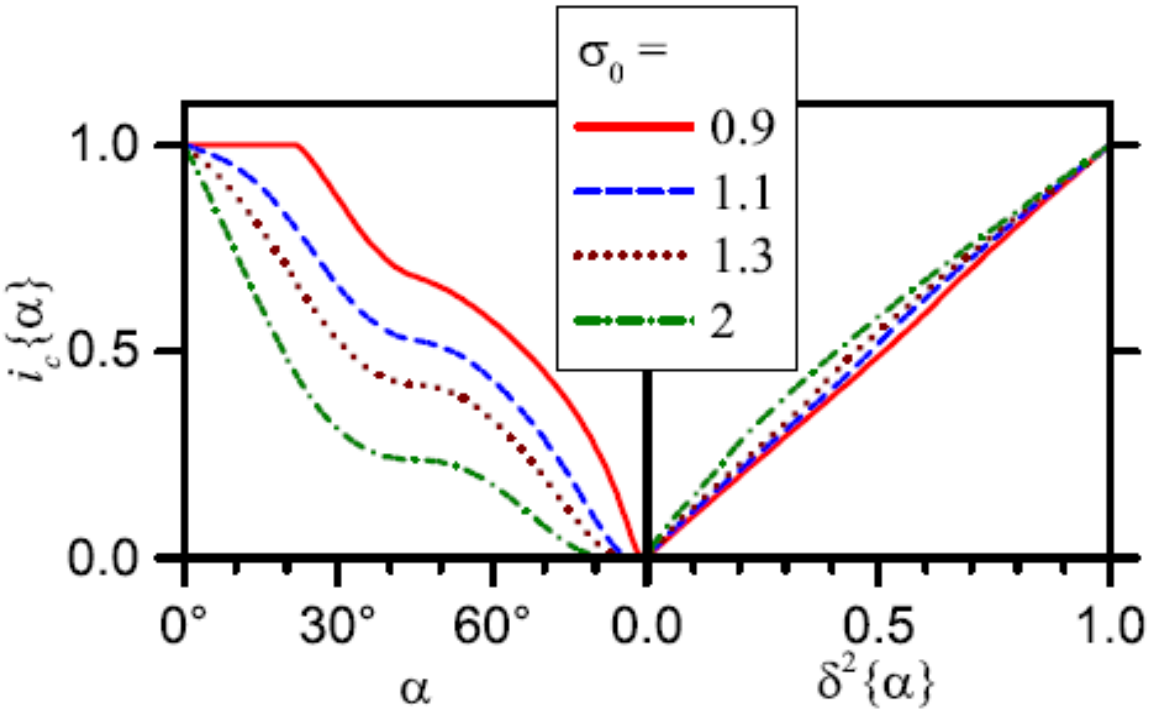

Proportionality between Josephson current and product of superconducting gaps: non-symmetric junctions involving d-wave superconductors with unidirectional CDWs (α as a driving force)

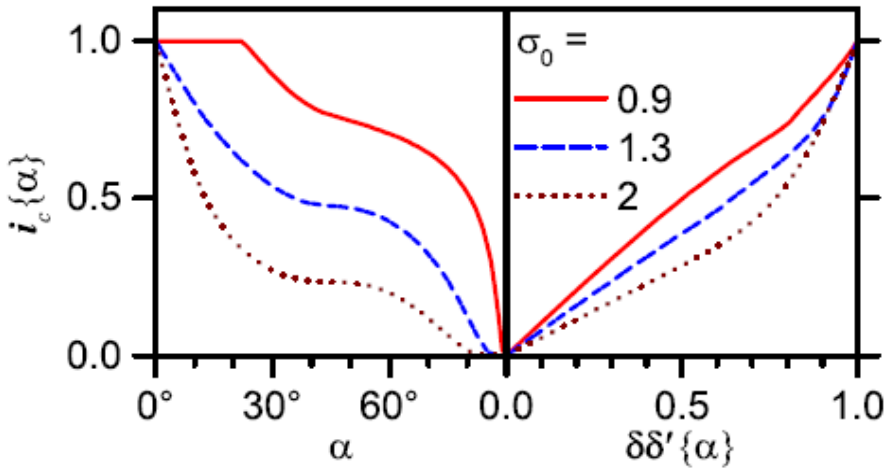

γ = 0°

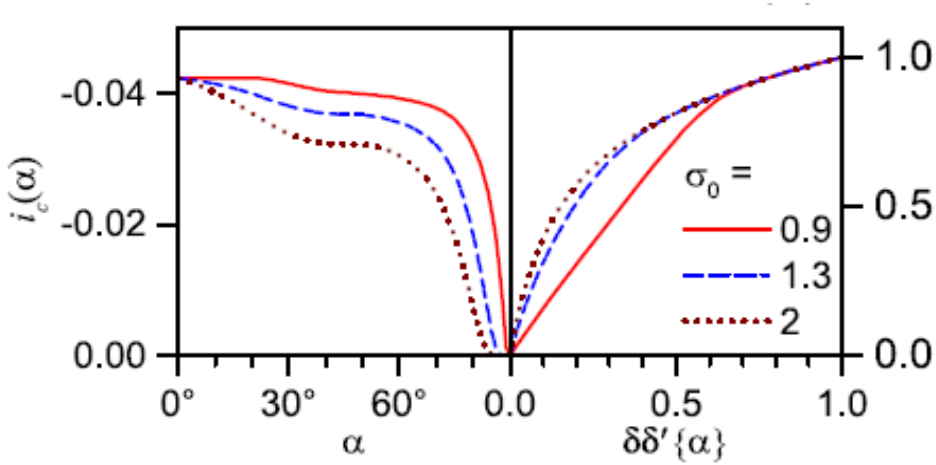

γ = 90°

Conclusions as for Josephson tunneling

- 1. CDWs can conspicuously alter angular dependences of the stationary Josephson currents.
- 2. Angular and doping current dependences are essentially different for various possible superconducting order parameter symmetries
- 3. Angular and doping current dependences are essentially different for checkerboard and unidirectional CDWs
- 4. CDWs violate proportionality between parameter-dependent Josephson current and product of left-hand-side and right-hand-side superconducting gaps
- 5. Josephson current measurements can supplement photoemission and tunnel spectroscopic studies to elucidate superconducting order parameter symmetry, detect CDWs and find their configuration